

Stainless steel as bipolar plate material for polymer electrolyte membrane fuel cells

Heli Wang, Mary Ann Sweikart, John A. Turner*

National Renewable Energy Laboratory, 1617 Cole Blvd., Golden, CO 80401, USA

Received 23 December 2002; accepted 31 December 2002

Abstract

Due to their low cost, high strength, ease of machining and shaping into thin sheets, as well as their corrosion resistance, stainless steels are considered to be good candidates for bipolar plate materials for the polymer electrolyte membrane fuel cell (PEMFC). We have tested several stainless steels in simulated PEMFC environments for application as bipolar plates. The results showed that the chromium content in the steel alloys has an important influence on the anodic behavior. The interfacial contact resistance of the carbon paper/stainless steel interface has been evaluated. Both tests show that 349TM is the best candidate for this application. When 349TM stainless steel was polarized in simulated PEMFC environments, it was found that stable passive films formed within 30 min. The interfacial contact resistance between the carbon paper and stainless steel increased due to the formation of the passive film. However, as soon as a stable passive film is formed, the interfacial contact resistance stabilized.

Published by Elsevier Science B.V.

Keywords: Bipolar plate; Stainless steel; Passive film; Polymer electrolyte membrane fuel cell; Corrosion

1. Introduction

Fuel cells are devices that convert the chemical energy of a fuel directly into electrical energy. Unlike internal combustion engines there is no burning of the fuel and therefore no generation of airborne pollutants. Due to its high efficiency and cleanliness as a power source, polymer electrolyte fuel cells have attracted interest from government agencies, academia, scientific laboratories and industry [1–8]. In a typical fuel cell, hydrogen and oxygen react electrochemically at separate electrodes producing electricity, heat, and water.

Power specifications can be met by connecting a specific number of cells in series to generate the necessary voltage and by sizing the active area of the cells to obtain the amperage needed. The bipolar plate is a multi-functional component in a PEMFC stack. It provides the electrical connectivity from cell to cell, and it separates the reactive gases. On the anode side of the plate, hydrogen gas is consumed to produce electrons and protons, as in Eq. (1). The electrons are collected by the anode and the protons enter the electrolyte (oxidation of hydrogen). On the other

side of the plate, i.e. at the cathode side, oxygen gas combines with electrons from the cathode and protons from the electrolyte to produce water (reduction of oxygen), as in Eq. (2):



Bipolar plates must be electrically conducting, mechanically and chemically stable, made of low permeability materials, corrosion resistant, allow uniform reactant gas distribution and product removal, be of low cost and able to be easily machined or shaped. For transportation purposes, lightweight and low volume should be also considered. Early fuel cell stacks used machined graphite as bipolar plates. Graphite's high cost and the requirement for machining the flow fields as well as its brittleness are the biggest difficulties in using graphite for the large-scale market. Therefore, alternative materials to the bipolar plate have been investigated, including use of carbon composite materials [9,10], metals with a thin coating [6,8,11], Fe-based alloys and stainless steels [12–18]. Obviously, stainless steel plates are a strong possibility due to their relatively high strength, high chemical stability, wide range of choice, ease of mass production and low cost. Their high density can be mitigated by using thin sheets. In addition, to further

* Corresponding author. Tel.: +1-303-275-4270; fax: +1-303-275-3033.
E-mail address: john_turner@nrel.gov (J.A. Turner).

eliminate the cost of including a flow field on metals, a stainless steel screen has been proposed [2,19].

A potential disadvantage for stainless steel is its chemical instability in the fuel cell environment, especially when in direct contact with the acidic polymer electrolyte membrane. The corrosion product of the bipolar plate could poison the catalysts and decrease the efficiency of the cell. So, the contamination level in fuel cell environments of a specific stainless steel must be considered in the material selection for a bipolar plate. Another point of concern is the natural oxide film on the stainless steel surface [20,21]. Although this surface film will protect the bulk material from further corrosion, it will significantly affect the contact resistance between the bipolar plate and the electrode backing. Moreover, in a fuel cell environment, it is possible that the surface film formed in air may not protect the bulk substrate and then the stainless steel bipolar plate may undergo further corrosion. If the corrosion film thickens over time, the contact resistance would also increase over time. Candidate stainless steels have been tested and used as bipolar plates and it was determined that the corrosion rate is low [14,16,17]. The test results showed stable cell output for thousands of hours [13,14,16,17]. This suggests that the passive film on some stainless steels would not thicken, otherwise there would be an increasing loss of output of the fuel cell over time.

The selection criteria for such candidate stainless steels were mainly the Cr, Mo and N content in accordance with the pitting resistance equivalent [12]. Stainless steels: 316L, 310L and 904L, are good candidate bipolar plate materials with the performance order 904L > 310L > 316L [16]. By means of Auger electron spectroscopy (AES), it was found that the thickness of the passive film, around 3–5 nm thick, generally decreases with the alloying elements content [17]. Therefore, higher alloying content promotes a lower interfacial resistance. On the other hand, a Dutch group reported that some specific stainless steels showed superior performance to 316L and 904L [13,14]. However, the details of such specific steels were not given. It is important to note that there were some disagreements about the same stainless steels between these groups, which may be due to the differences in the pretreatment of the alloys, since the chemical composition of the alloy and the surface treatments affect the properties of passive film. So, the purpose of this report is to evaluate stainless steels in environments simulating the bipolar plate situation in a PEMFC application.

2. Experimental

2.1. Materials and electrodes

Stainless steels plates of 316L, 317L and 349TM were provided by J&L Specialty Steel Inc., while 904L was purchased from Metalmen Sales Inc. Their chemical compositions are listed in Table 1.

Regardless of the thickness, the alloy plates were cut into samples of 2.5 cm × 1.3 cm. The samples were polished with #600 grit SiC abrasive paper, rinsed with acetone, dried, and one side was connected to a copper wire by means of silver paint for the electrical connection. Then the side for electrical contact (backside) and the edges of the samples were covered with insulating epoxy, leaving one side exposed for electrochemical measurements. The sealing process was repeated to eliminate possible leakage.

2.2. Electrochemical

According to previous studies in the field [3,13,18], 1 M H₂SO₄ + 2 ppm F⁻ was selected as the solution in this study. Sulfuric acid was selected because the membranes are pretreated in sulfuric acid. The high concentration (1 M) simulated the direct contact of the bipolar plate with the highly acidic polymer electrolyte. Fluoride ions at the ppm level was chosen based on water analysis of a running PEMFC system [12,22]. Thus, the solution chosen in the present study represented an aggressive environment for a relatively short test time. Since the bipolar plates in PEMFCs will be exposed to hydrogen gas on one side and to air/oxygen on the other side, the solution was bubbled thoroughly either with hydrogen gas (simulated PEMFC anode environment) or with pressured air (simulated PEMFC cathode environment) prior to and during the measurements. To simulate the operation condition of PEMFCs, all the electrochemical experiments were conducted at 70 °C.

A conventional three-electrode system was used in the electrochemical measurements, in which a platinum sheet acted as the counter electrode, a saturated calomel electrode (SCE) as the reference electrode and the stainless steel sample as the working electrode. All the potentials are referred to the SCE except otherwise specified. A Solartron 1287 potentiostat controlled by a computer was utilized to conduct the electrochemical experiments. For linear sweep voltammetry measurements, samples were stabilized in

Table 1
Chemical compositions of stainless steels

Material	C	Cr	Ni	Mn	Mo	Si	N	Cu	Cb	Co	Fe
316L	≤0.028	16.20–16.80	10.10–10.30	1.70–1.95	2.03–2.25	0.45–0.65	0.020–0.040	≤0.50		≤0.500	Balance
317L	≤0.028	18.10–18.60	12.45–12.75	1.60–1.90	3.05–3.35	0.25–0.55	0.045–0.07	≤0.50			Balance
904L	0.011	20.48	24.59	1.53	4.5	0.46		1.4			Balance
349 TM	0.05	23	14.5	1.5		1.4	0.13		0.40		Balance

solution at open circuit for 5 min then the scan was started from this open circuit potential in the anodic direction. A scanning rate of 1 mV/s was selected.

To investigate the performance of the candidate steels under PEMFCs' operational conditions, potentiostatic experiments were conducted. In these measurements, samples were also stabilized at open circuit for 5 min then a specific potential was applied and the current–time curves were recorded. Two potentials were chosen for the tests: -0.1 V for the PEMFC anode environment (equivalent to $\sim 0.1 V_{\text{NHE}}$) and 0.6 V for the PEMFC cathode environment (equivalent to $\sim 0.8 V_{\text{NHE}}$). In the former situation the solution was sparged with hydrogen gas, and in the latter case the solution was sparged with air.

2.3. Interfacial contact resistance (ICR)

Davies' method [17] for measurement of the interfacial contact resistance (ICR) between stainless steel and carbon paper was modified. In our setup as shown in Fig. 1, two pieces of treated Toray conductive carbon paper (Electro-Chem Inc.) were sandwiched between the steel sample and two copper plates. Such carbon paper has been used as the electrode backing [15]. An electrical current (1.000 A), sourced by means of a Tektronix TM506, was provided via the two copper plates. By measuring the total voltage drop through this setup, while the compaction force was gradually increased, it was possible to calculate the total resistance dependency on the compaction force according to:

$$R = \frac{VA_s}{I} \quad (3)$$

where R is the electrical contact resistance, V the voltage drop through the setup, I the current applied and A_s the surface area. The compaction force was applied by means of a manual FGS-50H test stand (Shimpo Instruments) and the force was monitored with a DFS-100R digital force gauge (Shimpo Instruments).

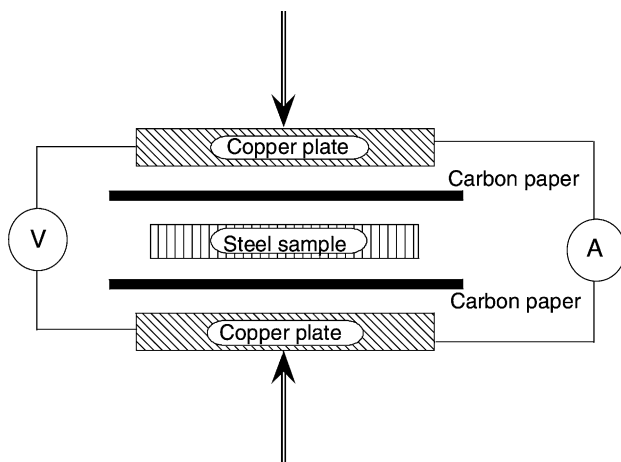


Fig. 1. Schematic of the test assembly for interfacial contact resistance.

As can be seen in Fig. 1, the total measured resistance is a sum of four interfacial components: two carbon paper/copper plate interfaces ($R_{\text{C/Cu}}$) and two carbon paper/surface film of stainless steel interfaces. To correct for the interfacial contact resistance between copper plate and carbon paper ($R_{\text{C/Cu}}$), a calibration was made in which only one layer of carbon paper was sandwiched between the two copper plates. This results in two carbon paper/copper plate interfaces and could be used to correct for the total measured resistance. After this correction, halving the result gives the interfacial contact resistance for the carbon paper/stainless steel ($R_{\text{C/SS}}$) interface (assuming the surfaces are homogeneous).

Different stainless steels were polished with #600 grit SiC abrasive paper and the interfacial contact resistance was investigated. All of these measurements were made using samples cleaned with acetone and dried with pressured nitrogen gas, and were carried out at room temperature.

When operating in a fuel cell the passive films may grow and thicken with time. So, the changes in the interfacial contact resistance against time for candidate steels at the operational condition were also evaluated. For these measurements, steel samples were pretreated potentiostatically in the solution for a specific period. Then the sample was unsealed and the backside was polished with #600 grit SiC abrasive paper, rinsed with acetone, and dried with pressured nitrogen gas. Then the total interfacial contact resistance was measured as above. With this approach, the measured total interfacial contact resistance will be a sum of a carbon paper/stainless steel ($R_{\text{C/SS}}$) interface component and a carbon paper/passive film interface component ($R_{\text{C/PF}}$).

3. Results and discussion

3.1. Polarization behavior of stainless steels

The anodic polarization curves for different stainless steels in 1 M $\text{H}_2\text{SO}_4 + 2$ ppm F^- at 70°C are shown in Figs. 2 and 3. In both figures, all of the steels investigated show passivation behavior, though such behavior is more apparent in Fig. 2 than in Fig. 3. The critical current, which is the peak current density for passivation, is the highest for 316L steel and the lowest for 349TM. In other words, the critical current decreases with the increasing Cr indicating that alloys with higher Cr content are easier to passivate. This can be related to the fact that Cr is the primary passivating element in stainless steels [20,21,23]. For all four stainless steels the passivation currents, which are the lowest current densities needed to maintain the passivation of the film, are all around $10 \mu\text{A}/\text{cm}^2$, little affected by the Cr content. This indicates that the passive films for these four steels are of the same nature.

Fig. 2 shows the results when the solution was sparged with hydrogen gas to simulate PEMFC anode environment. A very high critical current was registered for 316L. Again

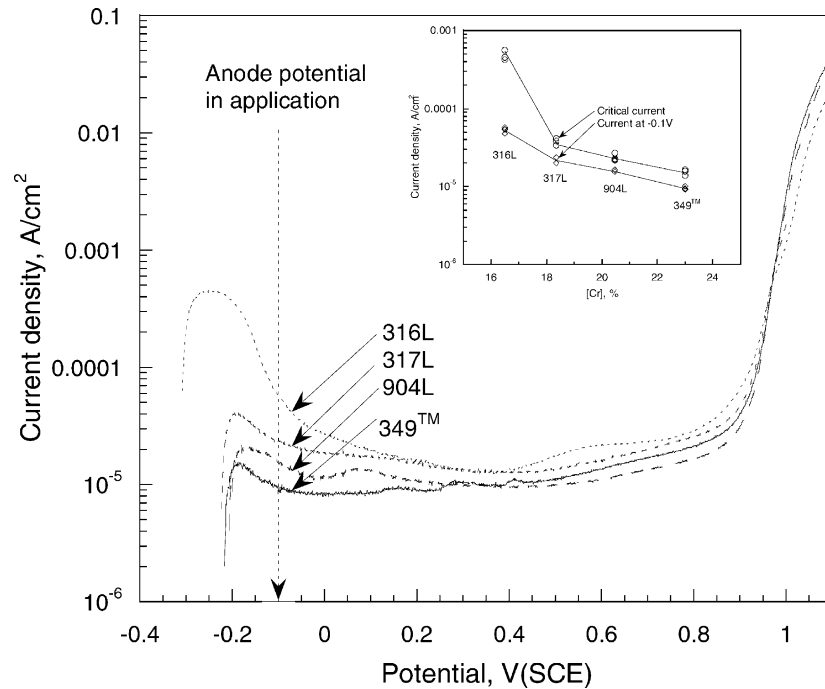


Fig. 2. Anodic behavior of stainless steels in 1 M $\text{H}_2\text{SO}_4 + 2 \text{ ppm F}^-$ at 70°C purged with H_2 . The anode potential in PEMFC application is marked. The inset shows the effect of Cr content of the alloys on the critical current and current density at -0.1 V in the solution.

the critical current decreases sharply with increasing Cr content in the alloys (see the inset). Higher Cr content makes the passivation easier. The anode potential under PEMFCs' operating conditions, which is around -0.1 V , is marked in the figure. And the current density at -0.1 V is plotted in the inset of Fig. 2. It is noticed that this anode potential is in the

passive region for all the materials tested. From the inset of Fig. 2, where the critical current and the current density at -0.1 V are plotted, it is seen that both currents decrease sharply with the Cr content. In terms of the performance in the anode environment for a PEMFC application, the materials are in the order of $349^{\text{TM}} > 904\text{L} > 317\text{L} > 316\text{L}$.

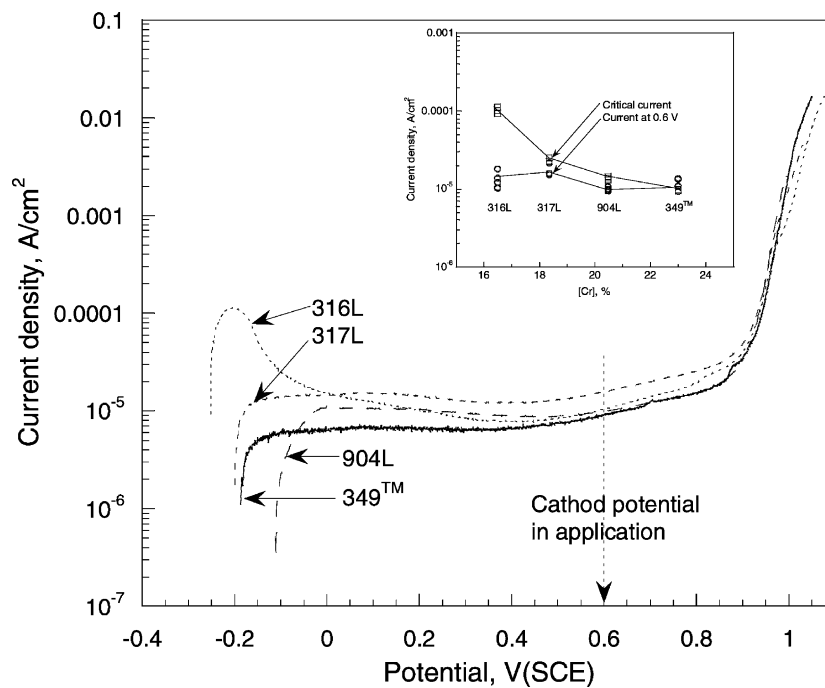


Fig. 3. Anodic behavior of stainless steels in 1 M $\text{H}_2\text{SO}_4 + 2 \text{ ppm F}^-$ at 70°C purged with air. The cathode potential in PEMFC application is marked. The inset shows the effect of Cr content of the alloys on the critical current and current density at 0.6 V in the solution.

Fig. 3 shows the results when solution was sparged with air to simulate the PEMFC cathode environment. Similarly, a high critical current was registered for 316L, and the critical current decreases with increasing Cr content in the alloys. Both the critical current and the passivation current for all the steels in Fig. 3 are lower than those in Fig. 2, indicating the beneficial effect of air in the formation and maintenance of these passive films. The cathode potential in PEMFCs' operation condition, which is around 0.6 V, is marked in the figure. Certainly, this potential is in the passive region for all the materials tested. The critical current and the current density at 0.6 V are plotted against Cr content and shown in the inset of Fig. 3. It is seen that critical currents decrease sharply with the Cr content, similar to the case in Fig. 2, but with a much lower gradient, while the current density at 0.6 V is not affected by the Cr content. In terms of the performance in cathode environment for PEMFC application, the materials are in the order of $349^{\text{TM}} > 904\text{L} > 317\text{L} > 316\text{L}$.

The above data gives the performance order of $349^{\text{TM}} > 904\text{L} > 317\text{L} > 316\text{L}$. 349^{TM} seems to be the best candidate for both anode and cathode environments in PEMFC applications.

Comparing the insets of Figs. 2 and 3, it is noticed that there is a fast decay in the current density at -0.1 V under anodic conditions, while the current density at 0.6 V under cathodic conditions is not affected. In the former case, the potential is just above the critical potential for passivation, thus the material's ability to passivate will have a strong influence on the current.

3.2. Interfacial contact resistance

The interfacial contact resistance between fresh samples of the different stainless steels and the carbon paper was investigated at different compaction forces. The results are shown in Fig. 4. Only one interfacial contact resistance of the carbon paper/surface film for stainless steel formed in air ($R_{\text{C/SS}}$) is plotted in Fig. 4, since both sides of the steel samples were polished to the same grade of abrasive paper and only the surface film formed in air on the stainless steels is present. It is found that the interfacial contact resistances are similar for the different steels. This may be related to the similarity of the surface film formed in air. In general, the interfacial contact resistance decreases slightly with the Cr content of the alloys, with 349^{TM} showing the lowest interfacial contact resistance and 316L the highest. This again, may be due to the Cr contribution to the surface film formed in air. The inset of Fig. 4 shows more clearly the interfacial contact resistances for different steels at a compaction force of 140 N/cm^2 . At such a compaction force, the interfacial contact resistance is of the order of $100\text{--}160 \text{ m}\Omega \text{ cm}^2$, decreasing with increasing Cr content in the alloys. The interfacial contact resistance between carbon paper and surface film formed in air for different steels ($R_{\text{C/SS}}$) is of the order of $349^{\text{TM}} < 904\text{L} < 317\text{L} < 316\text{L}$, which gives a surface conductivity order of $349^{\text{TM}} > 904\text{L} > 317\text{L} > 316\text{L}$. This result is in good agreement with previous results [12,15–17]. Moreover, our results for the interfacial contact resistance are in good agreement with previous investigations [17,18]. The result of less than $100 \text{ m}\Omega \text{ cm}^2$ from the Dutch group is

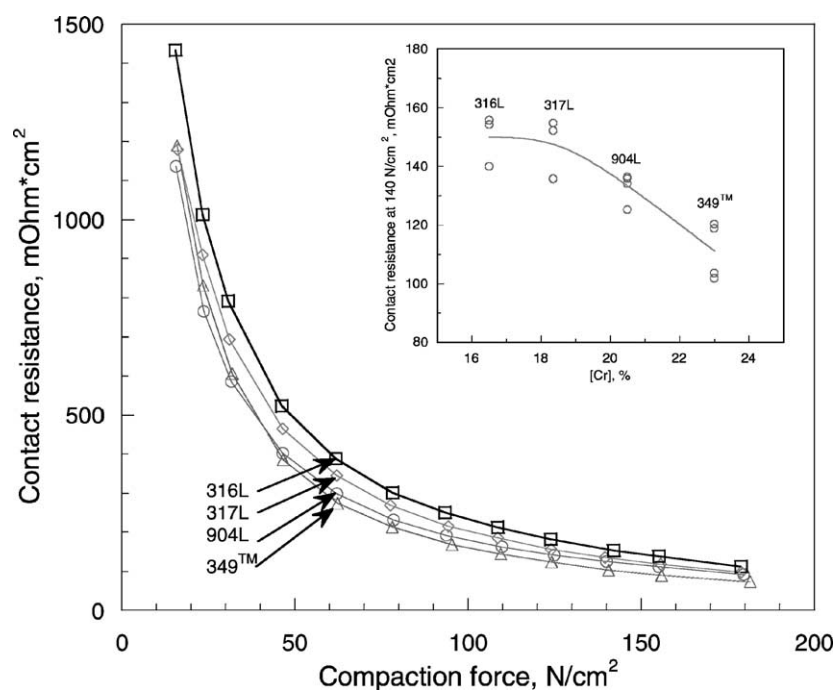


Fig. 4. Interfacial contact resistances for different stainless steels and carbon paper at different compaction forces. The inset shows the interfacial contact resistances for different steels at a compaction force of 140 N/cm^2 .

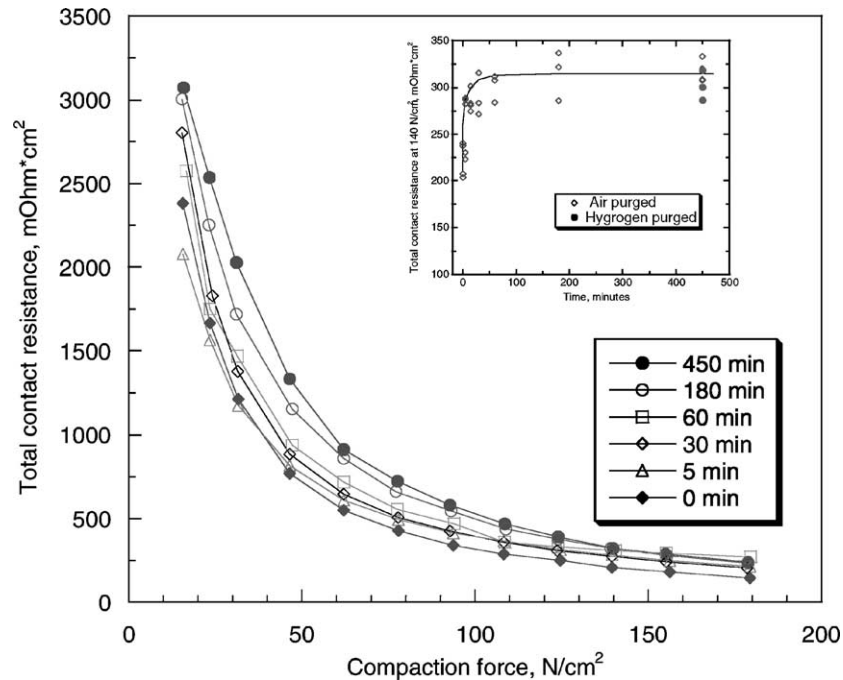


Fig. 5. Effect of the pretreatment time on the interfacial contact resistance between the passive film and carbon paper. The inset shows this effect at a compaction force of 140 N/cm².

due to the higher compaction force that was applied in those experiments [13,14]. Since 349TM showed the best behavior in the above experiments, 349TM was selected for further tests in the simulated anode and cathode environments of PEMFC operation.

While operating in the cathode environment of a PEMFC, the material can be easily passivated (Fig. 3). The major concern for 349TM then would be the possibility of additional film growth and its possible effect on the contact resistance. So, the contact resistance between the carbon paper and stainless steel was measured for steel samples pretreated under potentiostatic condition at 0.6 V for different periods of time. The results are shown in Fig. 5 in which results from fresh samples are also plotted. In these tests, one side of the sample was pretreated in the solution and this side is covered with the passive film formed under potentiostatic conditions. The backside of the sample is only covered with a normal surface film formed in air. It should be mentioned that Fig. 5 plots the total contact resistance of the two components: the interface of carbon paper/stainless steel with a film formed in air ($R_{C/SS}$) and the interface of carbon paper/passive film pretreated in solution ($R_{C/PF}$). In general, the total interfacial contact resistance for 349TM increases with increasing time in the cathodic environment. Similar behavior has been seen for 316L and 310L stainless steels [16,17]. The effect of the cathode environment is significant in the beginning of the treatment, especially at higher compaction force. The higher compaction force is of interest since it is used for PEMFC applications [16]. However, the effect decreases with prolonged time at the cathode potential. The inset of Fig. 5 shows the influence of

time on the total interfacial contact resistance at a compaction force of 140 N/cm². There is a rapid increase of the total resistance until around 15–30 min. This period can then be considered as the formation period of the passive film at that potential, which is in agreement with the potentiostatic measurements (see below). It then remains at around 320 mΩ cm², almost independent of the treatment time at 0.6 V. Referring to the inset of Fig. 4, where the interfacial contact resistance of carbon paper/349TM stainless steel at 140 N/cm² is around 120 mΩ cm², the interfacial contact resistance of carbon paper/349TM passive film ($R_{C/PF}$) would be around 200 mΩ cm². This is due to the fact that the surface film formed in air is thinner than the passive film formed at an applied anodic potential. The thin film formed in air may not protect the substrate from further corrosion. So, at the applied anodic potential passive film will develop and thicken. When the passive film is thick enough, further oxidation of the substrate is blocked and so the thickness of the passive film is expected to remain constant. Therefore, we will have a contact resistance as shown in the inset of Fig. 5. The inset of Fig. 5 also gives the interfacial contact resistance for samples treated in hydrogen gas purged solutions. Similar results for the interfacial contact resistance support the suggestion that the passive film formed in the first half hour of treatment determines the interfacial contact resistance. This behavior is beneficial to practical PEMFC operation, since after initial film formation, the thickness of the passive film should not increase significantly. It should be mentioned that all the interfacial contact resistances were measured with dry samples. In a practical situation where water is produced in the PEMFC and the

membrane is wet, the interfacial contact resistance should decrease.

3.3. Potentiostatic measurements for 349TM

The anode reaction in PEMFCs is hydrogen oxidation. So, the major concern for the material in this environment would be its corrosion resistance behavior and the film stability. Since the anode operating potential of around -0.1 V is close to the open circuit potential (Fig. 2) for 349TM in 1 M $\text{H}_2\text{SO}_4 + 2$ ppm F^- solution at 70°C , the steel may undergo a film dissolution at this potential. So, potentiostatic measurements for 349TM samples in solution purged with hydrogen gas were conducted at -0.1 V. The current–time behavior of this stainless steel is shown in Fig. 6.

From Fig. 6, it is seen that the transient current decays rapidly in the beginning. Then the current stays at a very low level, close to zero. Similar results were reported for 316L stainless steel in a solution of pH 1 at 80°C [24]. Again, the fast decay of the current is related to the passive film formation process. As soon as the whole surface is covered, the current needed to maintain the passivation is very low. Then, the current undergoes a positive–negative change. The inset of Fig. 6 shows this more clearly. This transfer occurs when the charge is in its maximum, which is approximately 20 min after the sample was biased at -0.1 V. A cathodic current (negative current) here indicates that the film is cathodically protected, possibly combined with hydrogen generation. So, under these conditions with cathodic current flow there would be no more active dissolution of the film. From Fig. 6, it is seen that the current is relatively steady

during the testing, indicating that the passive film maintained its stability very well.

The cathode reaction in PEMFCs is oxygen reduction and so the environment is oxidative. Potentiostatic measurements were carried out at 0.6 V in solution purged with air. Typical passivation behavior is shown in Fig. 7. The current tendencies in Figs. 6 and 7 are the same. Similarly, passivation occurred in a short period of time, and the current stabilized very quickly and stayed at a very low level, close to zero. Moreover, the current curve in Fig. 7 indicates that the passive film is very stable under the cathode condition. Comparing Fig. 7 with Fig. 6, it is seen that the current does not change from anodic to cathodic. This might be related to the fact that the applied potential is in the middle of the passivation region. The inset of Fig. 7 shows the beginning stage of the passivation, in which the charge passed during passivation is also plotted. There is a fast increase of charge in the beginning followed by a linear charge–time relation. The transition between the two different behaviors is at around 15 min of treatment time. Referring to the current curve, the current is kept in a very low level after 15 min of polarization at 0.6 V. So, it is reasonable to consider the first 15 min is the passive film formation period, or the passivation time. The time scale here is in excellent agreement with the measurements of the interfacial contact resistance (Fig. 5). Comparing the insets of Figs. 5–7, we may conclude that the passive film formed in the first 15–20 min at an anodic potential determines the interfacial contact resistance of the carbon paper/passive film interface. In addition, the passivation process with air purge occurred faster than that with hydrogen gas purge.

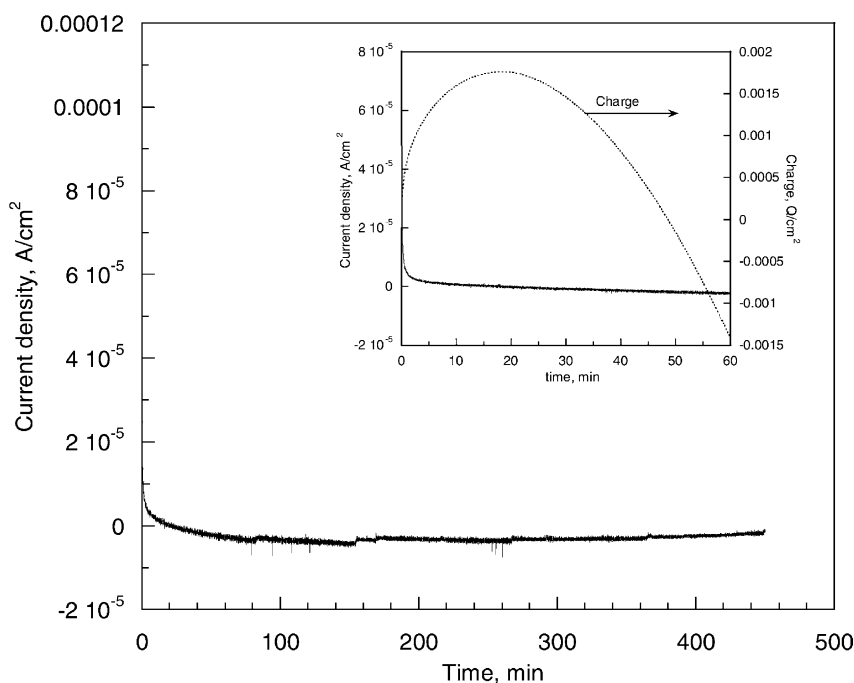


Fig. 6. Transient current and accumulated charge of 349TM stainless steel at -0.1 V in 1 M $\text{H}_2\text{SO}_4 + 2$ ppm F^- at 70°C purged with hydrogen gas. Inset shows the transient current and charge in the first hour.

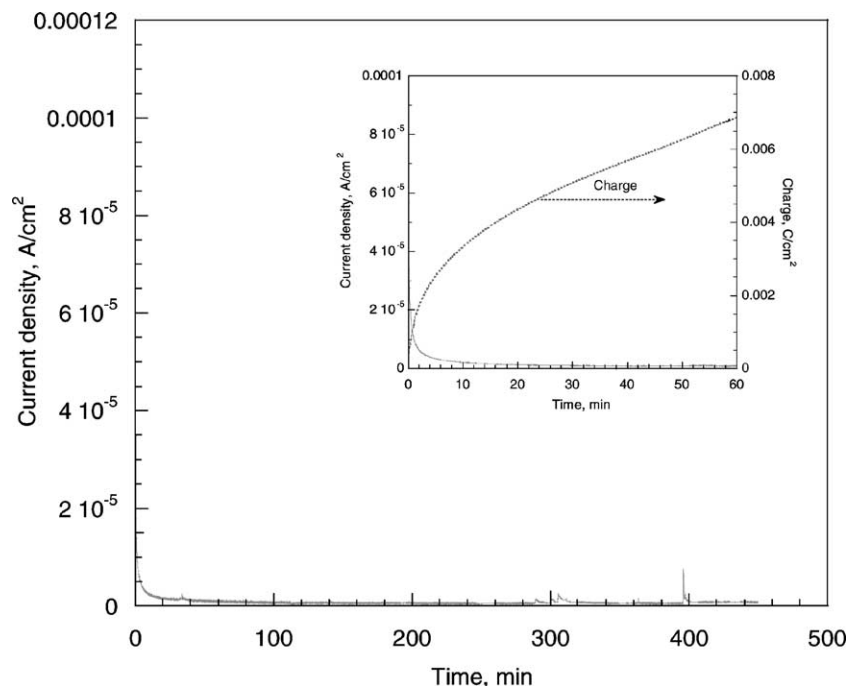


Fig. 7. Transient current and accumulated charge of 349TM stainless steel at 0.6 V in 1 M H₂SO₄ + 2 ppm F⁻ at 70 °C purged with pressured air. Inset shows the transient current and the charge in the first hour.

According to the above results, 349TM appears to be the best candidate stainless steel among the ones that were studied for a PEMFC bipolar plate application. Therefore, PEMFC stacks with such bipolar plates are now under construction in this laboratory and the material will be investigated under real operating conditions. Further test results will be reported.

4. Conclusions

Different stainless steels have been investigated in 1 M H₂SO₄ + 2 ppm F⁻ at 70 °C purged either with hydrogen gas or pressurized air to simulate an aggressive bipolar plate condition in a PEMFC environment. Both linear sweep voltammetry and interfacial contact resistance measurements indicated that the performance of the steels improved with the increase in the chromium content in the alloy, with 349TM being the best candidate for the application.

Stainless steel 349TM showed a very low critical passivation current in the solution purged either with hydrogen gas or with air. A stable passive film was formed within 20 min at -0.1 V in the simulated PEMFC anode environment. A stable passive film was also formed within 15 min at 0.6 V in the simulated PEMFC cathode environment. During the initial 15–30 min of polarization at 0.6 V, the interfacial contact resistance between the carbon paper and passive film increased with time. While for polarization times in excess of 30 min at 0.6 V, the interfacial contact resistance did not change much, which is encouraging for PEMFC applications. This suggests that the thickness of passive film

remains constant. This time scale is in agreement with the passive film formation process at 0.6 V.

Acknowledgements

The authors wish to thank Mr. James Halliday from J&L Specialty Steel Inc. for the stainless steels samples. This work was supported by the Hydrogen, Fuel Cell and Infrastructure Technologies Program of the US Department of Energy.

References

- [1] B.C.H. Steele, A. Heinzel, *Nature (London)* 414 (2001) 345.
- [2] S.J.C. Cleghorn, X. Ren, T. Espringer, M.S. Wilson, C. Zawodzinski, T.A. Zawodzinski, S. Gottesfeld, *Int. J. Hydrogen Energy* 22 (1997) 1137.
- [3] D. Chu, R. Jiang, *J. Power Sources* 80 (1999) 226.
- [4] J. Ihonen, F. Jaouen, G. Lindbergh, G. Sundholm, *Electrochim. Acta* 46 (2001) 2899.
- [5] C.E. Borroni-Bird, *J. Power Sources* 61 (1996) 33.
- [6] K.B. Prater, *J. Power Sources* 61 (1996) 105.
- [7] W. Smith, *J. Power Sources* 86 (2000) 74.
- [8] O.J. Murphy, A. Cisar, E. Clarke, *Electrochim. Acta* 43 (1998) 3829.
- [9] D. Busick, M. Wilson, in: D.H. Doughty, L.F. Nazar, M. Arakawa, H.-P. Brack, K. Naoi (Eds.), *New Materials for Batteries and Fuel Cells*, Proceedings of the Symposium of Materials Research Society, vol. 575, Materials Research Society, USA, 2000, 247 pp.
- [10] J. Scholta, B. Rohland, V. Trapp, U. Focken, *J. Power Sources* 84 (1999) 231.
- [11] D.R. Hodgson, B. May, P.L. Adcock, D.P. Davies, *J. Power Sources* 96 (2001) 233.
- [12] R. Hornung, G. Kappelt, *J. Power Sources* 72 (1998) 20.

- [13] R.C. Makkus, A.H.H. Janssen, F.A. de Bruijn, R.K.A.M. Mallant, *Fuel Cells Bull.* 3 (2000) 5.
- [14] R.C. Makkus, A.H.H. Janssen, F.A. de Bruijn, R.K.A.M. Mallant, *J. Power Sources* 86 (2000) 274.
- [15] P.L. Hentall, J.B. Lakeman, G.O. Mepsted, P.L. Adcock, J.M. Moore, *J. Power Sources* 80 (1999) 235.
- [16] D.P. Davies, P.L. Adcock, M. Turpin, S.J. Rowen, *J. Power Sources* 86 (2000) 237.
- [17] D.P. Davies, P.L. Adcock, M. Turpin, S.J. Rowen, *J. Appl. Electrochem.* 30 (2000) 101.
- [18] J. Scholta, B. Rohland, J. Garche, in: P.R. Roberge (Ed.), *Proceedings of the Second International Symposium on New Materials for Fuel Cell and Modern Battery Systems*, Ecole Polytechnique de Montreal, Canada, 1997, 300 pp.
- [19] M.S. Wilson, C. Zawodzinski, Fuel cell with metal screen flow field, US Patent no. 6,037,072 (2000).
- [20] M.G. Fontana, N.D. Greene, *Corrosion Engineering*, 2nd ed., McGraw-Hill, New York, USA, 1978, 163 pp.
- [21] H.H. Uhlig, R.W. Revie, *Corrosion and Corrosion Control: An Introduction to Corrosion Science and Engineering*, 3rd ed., Wiley, New York, USA, 1985, 78 pp.
- [22] R.L. Borup, N.E. Vanderborgh, in: *Proceedings of the Symposium of Material Research Society*, vol. 393, Materials Research Society, USA, 1995, 151 pp.
- [23] L.L. Shreir, *Corrosion: Corrosion Control*, vol. 2, 2nd ed., Butterworths, London, UK, 1978, pp. 11–113.
- [24] L. Ma, S. Warthesen, D.A. Shores, *J. New Mat. Electrochem. Syst.* 3 (2000) 221.